DIFFRACTION GRATING STRUCTURES IN SOLAR CELLS

Saleem H. Zaidi[1], James M. Gee[2], and Douglas S. Ruby[2]
[1]Gratings, Inc., Albuquerque, NM 87107
[2]Sandia National Laboratories, Albuquerque, NM 87185-0752

ABSTRACT

Sub-wavelength periodic texturing (gratings) of crystalline-silicon (c-Si) surfaces for solar cell applications can be designed for maximizing optical absorption in thin c-Si films. We have investigated c-Si grating structures using rigorous modeling, hemispherical reflectance, and internal quantum efficiency measurements. Model calculations predict almost ~ 100 % energy coupling into obliquely propagating diffraction orders. By fabrication and optical characterization of a wide range of 1D & 2D c-Si grating structures, we have achieved broadband, low (~ 5 %) reflectance without an anti-reflection film. By integrating grating structures into conventional solar cell designs, we have demonstrated short-circuit current density enhancements of 3.4 and 4.1 mA/cm^2 for rectangular and triangular 1D grating structures compared to planar controls. The effective path length enhancements due to these gratings were 2.2 and 1.7, respectively. Optimized 2D gratings are expected to have even better performance.

INTRODUCTION

In most c-Si photovoltaic modules, 50 % of the cost is associated with the c-Si wafer [1]. Therefore, a highly effective approach aimed at cost reduction in crystalline and multi-crystalline c-Si solar cells is better material utilization by using thinner (~ 1-20 μm) films. Reduced film thickness is also attractive due to lower bulk recombination and increased open-circuit voltages provided complete optical confinement can be achieved [2]. c-Si is strongly absorptive in the UV-visible spectral region. However, in near IR region (~ 0.8-1.1 μm) and particularly near the band edge, the absorption is weak; e.g. the absorption depth is ~ 100 μm at λ ~ 1 μm [3]. This weak absorption fundamentally limits the performance of thin-film c-Si solar cells. Surface texturing schemes aimed at enhancing near IR absorption by oblique optical coupling into the semiconductor have been extensively investigated [4]. Surface structuring schemes based on geometrical optics considerations may have limited applicability in thin films due to texture dimension approaching the film thickness.

A periodically textured surface such as a grating structure can be used to enhance absorption in thin films. Sheng, et al. first proposed this for thin film a-Si solar cells [5]. Using a waveguide configuration, it was shown that an appropriately designed grating structure can enhance short-circuit current by ~ 4-6 mA/cm^2 in comparison with a planar surface. Heine and Morf investigated diffraction gratings in c-Si solar cells [6]. In their scheme, grating structures were designed for optimum coupling into obliquely propagating diffraction orders inside the semiconductor material. Broadband anti-reflection characteristics of grating structures have also been extensively investigated [7].

Here, we report on an investigation of sub-micrometer c-Si grating structures by modeling, hemispherical reflectance, and internal quantum efficiency measurements. This investigation will help in optimizing grating structures aimed at maximizing optical absorption in thin-film c-Si solar cell devices.

MODELING OF GRATING STRUCTURES

Light interaction with a grating structure is a complex function of several parameters including incident wavelength, angle, polarization, period, profile, duty cycle, and depth [8]. For solar cell applications, the front-surface grating should be designed to enhance infrared absorption by efficiently coupling of light into the modes that propagate nearly parallel to the surface while minimizing coupling into the normally propagating zero-order mode. Using commercially available GSOLVER^{TM} modeling software, we have investigated rectangular, triangular, and blazed grating structures.

Figure 1 is an example calculation. It shows the diffraction efficiency for both TE and TM-polarizations for normal incidence. The grating period was selected at 0.65 μm so that both first and second orders were propagating. Finer periods – e.g., d=0.32 μm, where only the two ±1-orders relatively weak energy coupling. For the TE-polarization, ~ 40% of the incident energy at 0.5 μm depth is coupled into the ±1-diffraction orders (propagating at ~ 30° with respect to the normal), and minimal energy is coupled into the ±2-diffraction orders (propagating at ~ 60° with respect to the normal). For TM-polarization, almost 80 % of the incident energy is coupled to the ±1 and ±2-diffraction orders. Similar calculations for triangular-profiled grating structure show that at TE-polarization, ~ 60% of incident energy is coupled into the ±1-diffraction orders and approximately 10% is coupled into the ±2-diffraction orders. At TM-polarization, ~ 80% of the energy is coupled into ±1-diffraction orders and ~ 10% into the ±2-diffraction orders. Finally, for the blazed grating profiles, nearly 100% of the incident energy is coupled into diffraction orders for the TE polarization. For TM-polarization, same behavior is seen with ~ 30% coupling into the +2-diffraction order. A comparison of the energy distribution

among diffraction orders for the three profiles reveals that the blazed grating structure couples more energy into the transmitted diffraction orders, but that coupling into the second order is comparable for the three grating structures. The rectangular profile shows the least energy transfer into diffraction orders.

In general, our calculations show that high diffraction efficiencies can be achieved as long as the propagation angle is ≤ 60° with respect to the surface normal. For higher propagation angles, most of the energy is coupled back into the normally propagating zero-order modes.
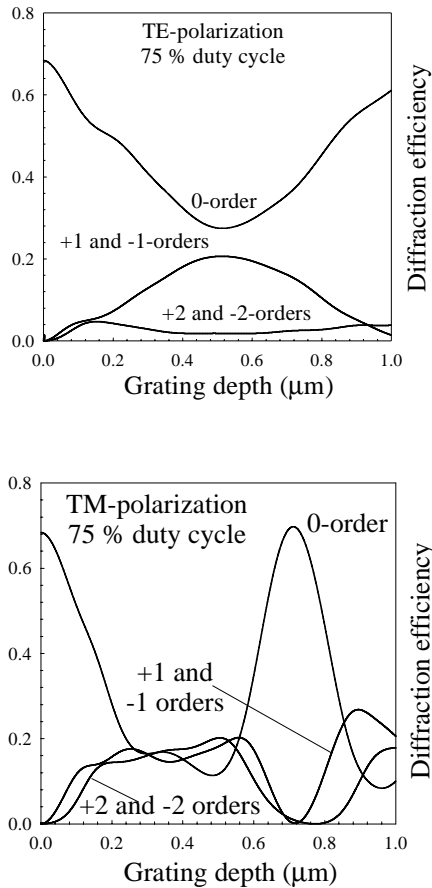

Figure 1. Diffraction efficiency calculations as a function of grating depth for symmetric rectangular profile grating structure at λ=1.0 μm.

FABRICATION OF GRATING STRUCTURES

We have developed low-cost, large-area inter-ferometric lithography techniques to pattern a wide range of 1D and 2D periodic structures [9]. Interference between two coherent laser beams produces a simple periodic pattern at d=λ/2sinθ, where λ is the exposure wavelength, and 2θ is the angle between the two inter-secting laser beams. For λ=355 nm, θ= 60°, periods down

to ~ 200-nm can be easily fabricated. Typically, grating structures are first formed in photoresist followed by pattern transfer to c-Si using an appropriate combination of wet and dry etching techniques. Figure 2 shows scanning electron microscope pictures of 1D triangular and rectangular profile gratings, and a 2D hole pattern etched in c-Si using RIE and wet-chemical etching methods [10]. The triangular structure shown in Fig. 2 is characterized by period of ~ 420 nm with full width at half-maximum depth of ~ 100 nm etched to a depth of ~ 600 nm. The rectangular profile grating shown in Fig. 1 has a period of 500 nm, linewidth of ~ 130 nm, and depth of ~ 1000 nm. The 2D hole pattern at 800-nm period is has a linewidth ~ 270 nm and depth of ~ 800 nm.
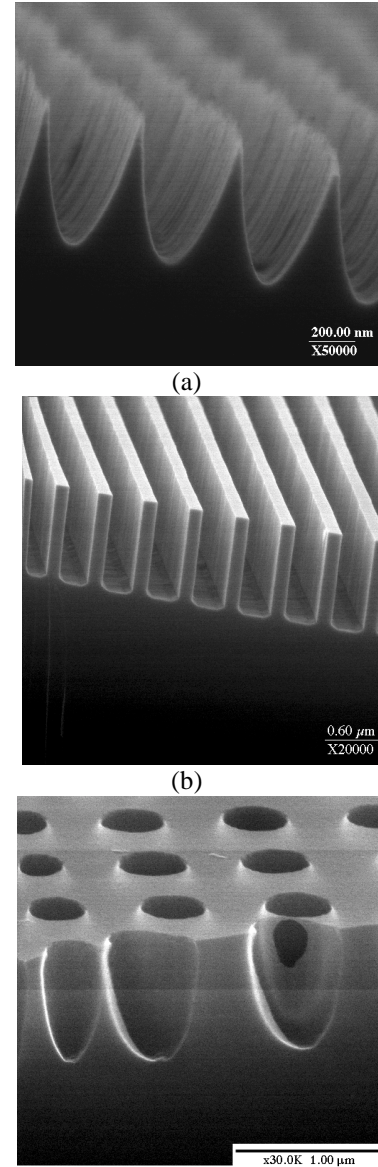

(a)

(b)

Figure 2. SEM photomicrographs of (a) 1D triangular, (b) 1D rectangular, and (c) 2D hole pattern grating.

Spectral reflectance measurements of grating structures were carried out using a Cary Model 5E (UV-VIS-NIR) spectrophotometer and a Labsphere (RSA-CA-

50) integrating sphere. Figure 3 shows absolute hemispherical reflectance measurements from grating structures shown in Fig. 2. It is seen that broadband reduced reflection is observed from the triangular grating profile. In contrast, the rectangular-profiled grating structure supports a number of narrow, low reflectance spectral bands. For the triangular profiles, the same broadband anti-reflection behavior is seen with both polarizations. For the rectangular profiles, these spectral bands are a critical function of the incident light polarization. For the 2D hole-pattern, a broadband anti-reflection behavior is observed. The reflection can be further reduced in all cases by application of anti-reflection films.
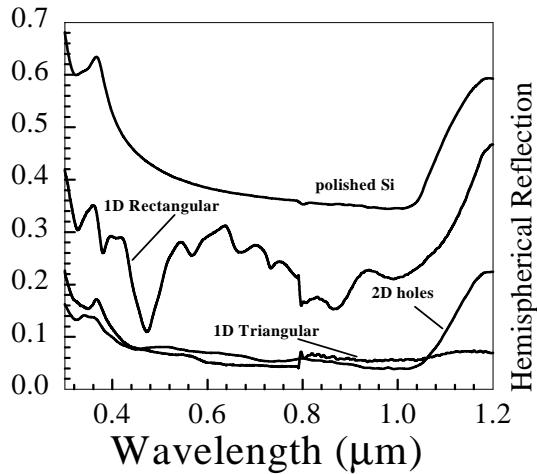

Figure 3. Hemispherical reflectance measurements from grating structures shown in Fig. 2. Reflectance from polished c-Si surface is shown for comparison.

INTERNAL QUANTUM EFFICIENCY MEASUREMENTS

Grating solar cells were fabricated on 4" diameter, p-type, 1 Ω-cm resistivity wafers at Sandia National Laboratories. Wafers were RIE textured with periodic patterns. The junction depth was ~ 0.5 μm on the planar region. A 10-nm thick passivating SiO_2 film was grown during back surface field formation at ~ 900 °C. For comparison, planar and grating regions of ~ 2x2 cm^2 were formed on each cell. Internal quantum efficiency measurements from planar and grating regions were acquired to understand the influence of grating structure on cell efficiency. The IQE measurements of triangular and rectangular profiled 1D gratings exhibited substantially reduced blue response. This was attributed to the lack of adequate passivation in the strongly absorptive grating region, and probably to some residual surface damage suffered from the RIE process. By incorporating RCA clean process prior to emitter formation, the blue response was significantly improved. Figure 4 shows the IQE response of a 1D rectangular profile grating structure. For comparison, the planar surface IQE adjacent to

the grating is also plotted. It is seen that the grating structure cell still exhibits lower IQE in 0.4-0.6-μm spectral region presumably due to residual RIE-induced surface damage. The IQE response, however, is significantly enhanced in the long wavelength region. The surface reflectance has also been significantly reduced.
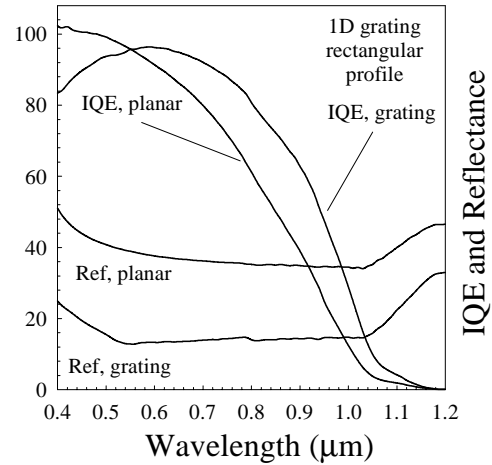

Figure 4. Internal quantum efficiency from 1D rectangular profile grating. For comparison, IQE response of planar surface is also shown.

Figure 5 shows similar IQE and reflectance measurements from a 1D triangular profiled grating structure. This grating structure exhibits slightly improved IQE response in the short wavelength region, but it is still lower than the planar surface. The enhancement in the long wavelength region is not as pronounced as for the rectangular profile.

We can eliminate the substrate variation by plotting IQE ratios from the grating and planar regions of the same wafer. Fig. 6 plots the IQE ratios for the rectangular and triangular profiled grating structures. It is seen that for the rectangular profile, the ratio is less than 1 for wavelengths < 0.55 μm, and the maximum enhancement of ~ 2.7 is observed at λ ~ 1.1 μm. For the triangular profile, the IQE ratio is less than 1 for wavelengths < 0.5 μm, while the maximum enhancement of ~ 1.6 is seen at λ ~ 1.1 μm. The IQE enhancement in the IR region can best be understood on the basis of the diffraction calculations presented earlier. The grating structure couples significant energy into the obliquely propagating diffraction orders inside c-Si. These transmitted diffraction orders generate electron-hole pairs closer to the surface, thus, enhancing the probability of collection by the junction.

ANALYSIS OF RESULTS

There is clearly an improvement in IQE due to the grating (Fig. 4-6). A convenient method to quantify

the effect of the grating alone on improving IQE is to analyze the inverse IQE versus absorption length [11]. The linear regime of this relationship in the near infrared region gives a measure of the internal collection length (L_{iqe} and Fig. 7). L_{iqe} is a function of the bulk material quality (e.g., bulk diffusion length) and the internal path length. Since the planar and grating regions were adjacent within the same cell and have very similar bulk properties, a ratio of L_{iqe} between the textured and planar regions gives the effective increase in path length due to the grating. We refer to "effective" path length enhancement since the generation profile with the grating is a combination of different modes traveling at different angles. The effective path length enhancement for the triangular and rectangular profiles is roughly 1.7 and 2.2, respectively. For comparison, the path length enhancement with chemically textured surfaces is around 1.3 since the light is coupled into the silicon at a well-defined angle [11].
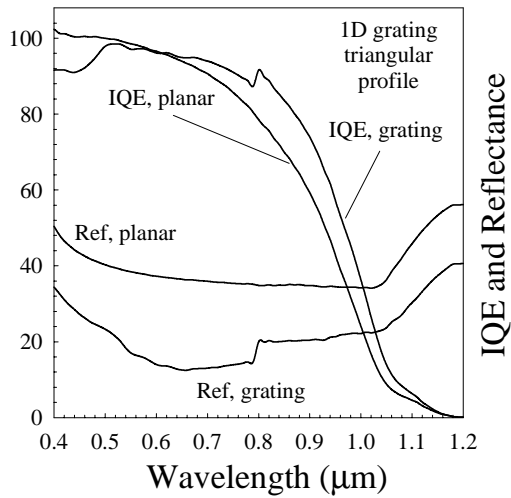
[3] M. A. Green and M. J. Keevers, Prog. in Photo. Research and Applications **3**, 189 (1995).
[4] P. Campbell and M. A. Green, Appl. Phys. Lett. **62**, 243 (1987).
[5] Ping Sheng, A. N. Bloch, and R. S. Stepleman, Appl. Phys. Lett. **43**, 579 (1983).
[6] C. Heine and R. H. Morf, Appl. Opt. **34**, 2476 (1995).
[7] D. H. Raguin and G. M. Morris, Appl. Opt. **32**, 1154 (1993).
[8] S. Kemme, S.H. Zaidi, and J. M. Gee, 9th Workshop on c-Si Mat. and Proc., Breckenridge (1999).
[9] Saleem H. Zaidi and S. R. J. Brueck, J. Vac. Sci. Technol. **B11**, 458 (1993).
[10] Saleem H. Zaidi, An-Shyang Chu, and S. R. J. Brueck, J. Appl. Phys. **80**, 6997 (1996).
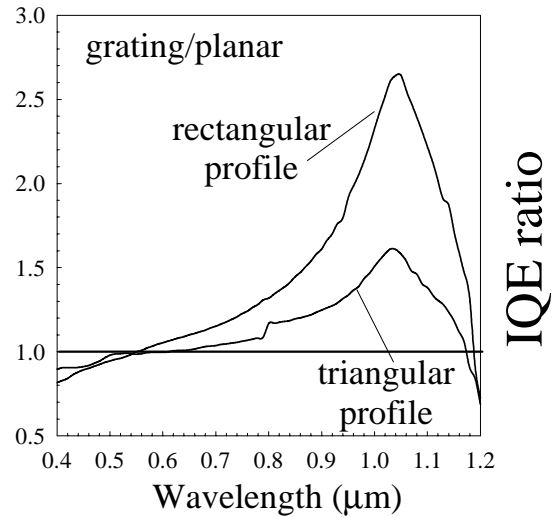[11] Paul A. Basore, 23rd IEEE Photo. Spec. Conf., 147 (1993).

Figure 5. Internal quantum efficiency from 1D triangular profile grating. For comparison, IQE response of planar surface is also shown.

Figure 6. Ratio of IQE response from grating to the planar surfaces for rectangular and triangular profiles.

REFERENCES

[1] A. Suzuki, M. Kaneiwa, T. Saga, and S. Matsuda, IEEE Trans. Elect. Dev., **ED-46**, 2126 (1999).
[2] T. Tiedje, E. Yablonovitch, G. D. Cody, and B. G. Brooks, IEEE Trans. Elect. Dev., ED-31, 711 (1984).
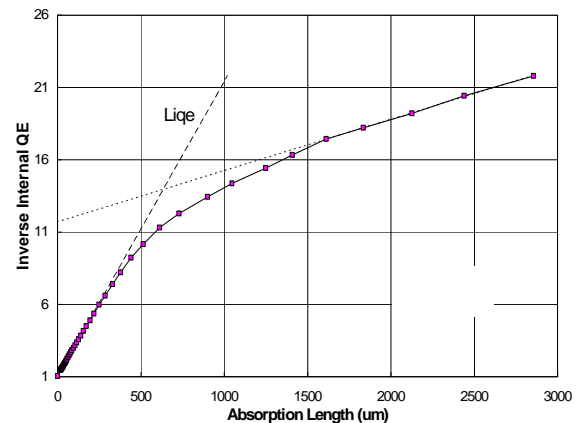
Figure 7. Plot of inverse-IQE versus photon absorption length for the planar cell of Fig. 5. L_{iqe} is the inverse slope of the initial linear regime [11].